

Asynchronous response of coupled pacemaker neurons

Ramana Dodla and Charles J. Wilson

Department of Biology, University of Texas at San Antonio, San Antonio, TX 78249

Abstract

We study a network model of two conductance-based pacemaker neurons of differing natural frequency, coupled with either mutual excitation or inhibition, and receiving shared random inhibitory synaptic input. The networks may phase-lock spike-to-spike for strong mutual coupling. But the shared input can desynchronize the locked spike-pairs by selectively eliminating the lagging spike or modulating its timing with respect to the leading spike depending on their separation time window. Such loss of synchrony is also found in a large network of sparsely coupled heterogeneous spiking neurons receiving shared input.

PACS numbers: 87.19.lm, 05.45.Xt, 87.19.1l

Phase locking or synchrony of oscillatory systems is a ubiquitous phenomenon in physics [1, 2], chemistry [3], and biology [4, 5]. The theory of weakly coupled oscillators predicts that phase-locking can arise from mutual interactions among oscillators [6, 7, 8, 9, 10, 11, 12, 13]. Phase locking is also facilitated by a common external input [14, 15] either with or without weak mutual interactions. But the theory of weakly coupled oscillators is strictly applicable only for oscillators with similar natural frequencies [16]. In some brain structures, there are mutually-interconnected oscillatory neurons with more frequency heterogeneity than allowed by the theory of weakly coupled oscillators [17]. Oscillators with substantially different natural frequencies may still become phase-locked if coupled strongly enough [18], but the influence of common inputs to these strongly coupled systems has not been fully explored [19, 20, 21, 22]. We are specifically motivated by studies of the subthalamic nucleus (STN) and globus pallidus (GP) which contain interconnecting oscillatory neurons that receive common inhibitory inputs. These neurons are normally uncorrelated but become strongly correlated in Parkinson’s disease [23]. In this Letter we construct oscillating two-neuron network models with different natural frequencies but that are phase-locked due to strong mutual interconnections. We show that a common external inhibitory input can reduce or abolish phase-locking and decorrelate their firing. The amount of decorrelation depends on the phase difference between the spike times in the phase-locked state.

Our results are demonstrated with coupled two-neuron networks that use three different models of varying complexity: a detailed neuron model that reflects realistic properties of the STN neurons including rebound currents, a reduced three-variable model (N+K) derived from the first model, and the generic Hodgkin Huxley (HH) neuron model, which was also used as a model of the GP neuron. The results are also extended to a larger network of 10 sparsely coupled neurons. We used a shared external inhibitory input, because both the GP and STN receive strong inhibitory inputs. Interconnections among neurons within the STN network model are excitatory, whereas the GP cells are coupled by inhibitory connections. Unlike integrate-and-fire type neuron models that may fail to synchronize for strong coupling [24] or for common input [14], our neuron pairs can display robust 1:1 phase-locking of spike times in the absence of external input. This kind of 1:1 phase-locking is sometimes also called linear synchrony [25, 26] in studies of coupled chaotic oscillators. Our study highlights the importance of the timing of the arriving inputs in decorrelating the phase-locked state. However, we confine our study to neuron models that are periodic and

are not chaotic.

We consider two coupled pacemaking model neurons at dissimilar frequencies ($\omega_{1,2}$) and affected by identical synaptic noise. The current balance equations (with unit membrane capacitance) are

$$\begin{aligned}\dot{V}_1 &= I_1 - I_g^1 - gS_2 \times (V_1 - E) - I_{\text{inh}}(V_1, t), \\ \dot{V}_2 &= I_2 - I_g^2 - gS_1 \times (V_2 - E) - I_{\text{inh}}(V_2, t),\end{aligned}$$

where $V_{1,2}$ are the membrane voltages. For mutual excitation, $E \equiv E_{\text{exc}} = 10$ mV and $g \equiv g_{\text{exc}}$, and for mutual inhibition $E \equiv E_{\text{inh}} = -85$ mV and $g \equiv g_{\text{inh}}$. I_j is a steady applied current. $j = 1, 2$ is the index of the neuron. All the three models were used with mutual excitation, and the HH model was also used with mutual inhibition. For the realistic STN model, $I_g^j \equiv I_g(V_j, n_j, h_j, r_j, [\text{Ca}]_j)$, is a function of V_j , potassium activation (n_j), sodium inactivation (h_j), low-threshold calcium inactivation (r_j), and calcium concentration ($[\text{Ca}]_j$) variables. These two equations along with those for n_j , h_j , r_j , and $[\text{Ca}]_j$, together describe the coupled system [36]. For the HH model, $I_g^j \equiv I_j(V_j, m_j, h_j, n_j)$, and the gating variables are given by standard equations [27] at $T = 0^\circ\text{C}$, $Q_{10} = 3^{(T-6.3)/10}$. A transformation $V \rightarrow -V - 60$ was used, and E_L was depolarized from -49.387 mV to -17 mV to trigger pacemaking. The N+K model is derived from the STN by setting rebound (G_T) and all other calcium dependent maximal conductances ($G_{\text{Ca}}, G_{\text{AHP}}$) to zero, and thus $I_g^j \equiv I_j(V_j, n_j, h_j)$. The conductance state variable, $S_{1,2} \equiv S(V_{1,2}, t)$ is noninstantaneous and depends on the time history of $V_{1,2}$ via a differential equation [28], and can range from 0, when the membrane is near rest, to 1 during an action potential [37]. This incorporates a mutual coupling time constant, $1/\beta$. $I_{\text{inh}}(V_j, t)$ is an inhibitory input current generated from alpha function conductances timed at random but identical Poisson process arrival times ($t_i, i = 1, \dots$) with rate λ_{inh} : $I_{\text{inh}}(V_j, t) = G_{\text{inh}} \sum_{t_i} \frac{t-t_i}{\tau_{\text{inh}}} e^{1-\frac{t-t_i}{\tau_{\text{inh}}}} H(t-t_i) \times (V_j - E_{\text{inh}})$. $G_{\text{inh}} = 0 - 1$ nS/ μm^2 for STN and N+K, and $0 - 1$ mS/ cm^2 for the HH network, and $\tau_{\text{inh}} = 1 - 10$ ms. A fourth order Runge-Kutta algorithm with $1 \mu\text{s}$ time step was used to integrate up to 1000 s. The spike time sequences (s_1 and s_2) of our networks, when they were not driven, are 1:1 phase-locked with spike separation t_w and thus fall in the (s_1, s_2) phase space on the diagonal line $s_1 = s_2$. The deviations from this linear synchrony (also see [25] and references there in) due to shared input are large and random. An asynchrony parameter that measures the fraction of such deviating spike times is defined: $A = 1 - N_{\text{sync}}/N_{\text{max}}$, where N_{sync} is the number of spike time

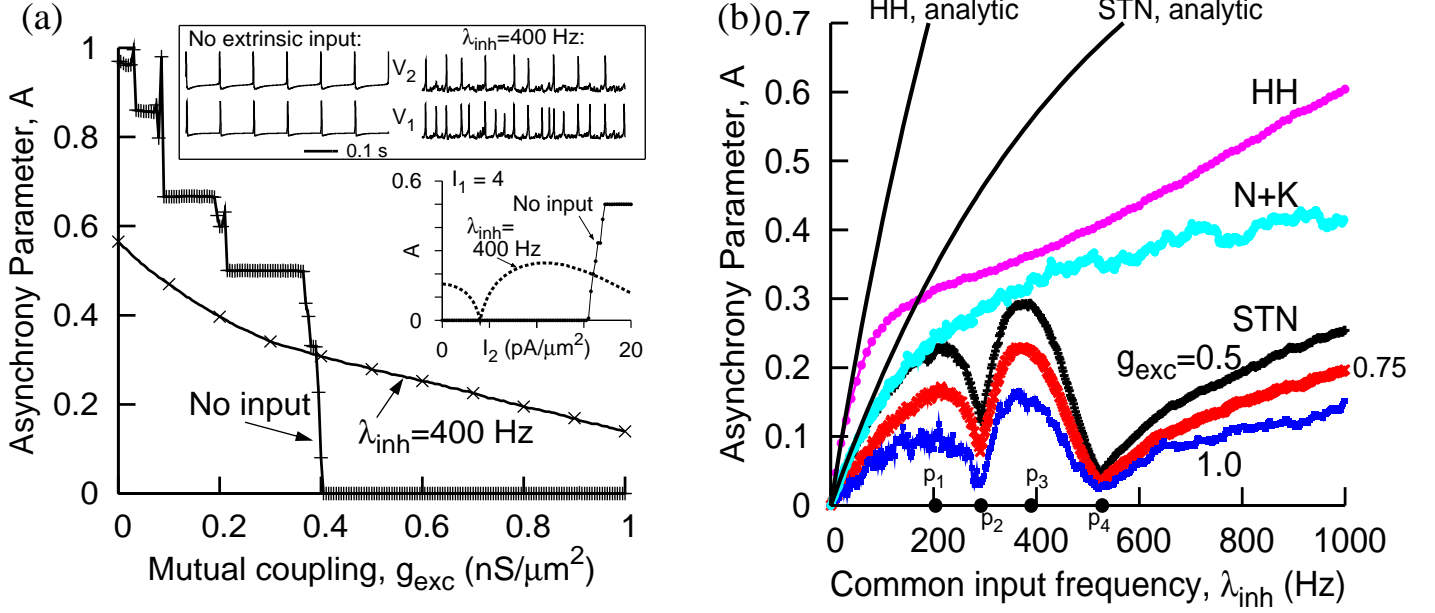


FIG. 1: Emergence of asynchrony for shared inhibition. (a) Coupled STN network. $\omega_1 = 2.7 \text{ Hz}$ ($I_1 = 0$) and $\omega_2 = 9.3 \text{ Hz}$ ($I_2 = 8 \text{ pA}/\mu\text{m}^2$). $G_{\text{inh}} = 1 \text{ nS}/\mu\text{m}^2$. $g_{\text{exc}}^* = 0.4 \text{ nS}/\mu\text{m}^2$. The top inset shows brief time courses at $g_{\text{exc}} = 0.5 \text{ nS}/\mu\text{m}^2$. For the same conductance parameters, the effect of frequency heterogeneity is shown in the bottom inset. (b) Frequency dependence of A for the three networks: STN ($G_{\text{inh}} = 1 \text{ nS}/\mu\text{m}^2$, and three different values of g_{exc}), N+K ($I_1 = 0$, $I_2 = 8 \text{ pA}/\mu\text{m}^2$, $g_{\text{exc}} = 0.62 \text{ nS}/\mu\text{m}^2$, $G_{\text{inh}} = 1 \text{ nS}/\mu\text{m}^2$), and HH ($I_1 = 0$, $I_2 = 8 \text{ pA}/\mu\text{m}^2$, $g_{\text{exc}} = 0.2 \text{ mS}/\text{cm}^2$, $G_{\text{inh}} = 1 \text{ mS}/\text{cm}^2$). p_1, \dots, p_4 mark input frequencies at which A changed its character in the STN network due to T-current activation, and are described in the text. ($\tau_{\text{inh}} = 1 \text{ ms}$).

pairs (one spike from each neuron) in a time window t_w and $N_{\text{max}} = \max\{N_1, N_2\}$, where $N_{1,2}$ are spike counts of the two neurons. $A = 0$ for 1:1 phase-locked state. For phase-locked states that have large t_w [in Fig. 3(b)], shorter separations also constitute deviations from the coherent state. Thus an asynchrony measure called inter spike interval (ISI) distance [29] defined as $\frac{1}{T} \int_0^T \frac{|s_1 - s_2|}{\max\{s_1, s_2\}} dt$ is used. The ISI-distance quantifies the jitter around the diagonal line, $s_1 = s_2$. However, both these measures give qualitatively similar results.

Figure 1(a) shows the results of two mutually excitatory STN neurons that have very different intrinsic spike frequencies. In the absence of external input, mutual coupling that exceeds a critical level (g_{exc}^*) phase-locks the spike times of both the neurons in 1:1 ratio. This causes A to become 0 as the frequencies of both the cells become identical. An example

of the voltage time courses in this state is shown in Fig. 1(a), top inset, left. When the external inhibitory input was turned on [Fig. 1(a), top inset, right], the spike times of both the cells became arrhythmic and the firing rates became different. The common input countered the effect of mutual coupling by decreasing the number of the 1:1 phase-locked spike pairs. The enhanced spike count resulted due to activation of low-threshold rebound calcium current (i.e. the T-current). But the loss of phase-locking is not dependent on the T-current activation (see results using the N+K network below). The result of the loss of the 1:1 phase-locking between the spike times is also seen as a finite non-zero value of A in the earlier phase-locked regime ($g > g_{\text{exc}}^*$). For this network, frequency heterogeneity is essential to elicit finite A . This is demonstrated in Fig. 1(a), bottom inset. In the absence of input, phase-locking was achieved for a wide range of frequency disparity. With inhibitory input, A became non-zero in this region except when the frequencies were identical ($I_1 = I_2$). The dependence of A on the input rate is shown in Fig. 1(b) for all the two-neuron coupled model networks with mutual excitation. In the absence of input (i.e. at $\lambda_{\text{inh}} = 0$), the networks were 1:1 phase-locked (i.e. $A = 0$). At an input rate of 1 kHz, about 40% of the locked spikes in the N+K network, and more than 50% of the locked spikes in the HH network became unpaired. But the STN network model exhibited frequency-dependent activation of its rebound current that led to a modulation of A . The T-current is most actively recruited in the slower neuron between p_1 and p_3 , and in the faster neuron between p_2 and p_4 . Thus, the firing rate as a function of λ_{inh} increased in both the neurons between p_2 and p_3 leading to an increasing A . Active recruitment in only one of the cells led to enhancement of phase-locking or reduction in A .

The loss of 1:1 phase-locking observed in the N+K, the HH, and the STN network (for $\lambda_{\text{inh}} < p_1$, hence no significant rebound spikes) emerges by selective elimination of one of the spikes in otherwise phase-locked spike pairs [see ISI histogram in Fig. 2(b) bottom inset]. Shared input cannot desynchronize the locked state if the spike pair separation $t_w = 0$. For small t_w , a brief synaptic input is needed for disruption of the locked state. t_w is determined by the dynamics of the synaptic coupling conductance ($S(V_j, t)$) and the coupling strength g_{exc} . It increases with frequency heterogeneity [Fig. 2(a)]. For the STN network, empirically, $t_w \sim a(g_{\text{exc}} - g_{\text{exc}}^*)^{-b}$, where $a = 0.78$, $b = 0.44$ away from the criticality (g_{exc}^*), and $a = 1.3$, $b = 0.2$ near criticality. An inhibitory stimulus event preceding a locked pair [Fig. 2(a) inset] may reduce the spike separation, but one or more events that are positioned appropriately

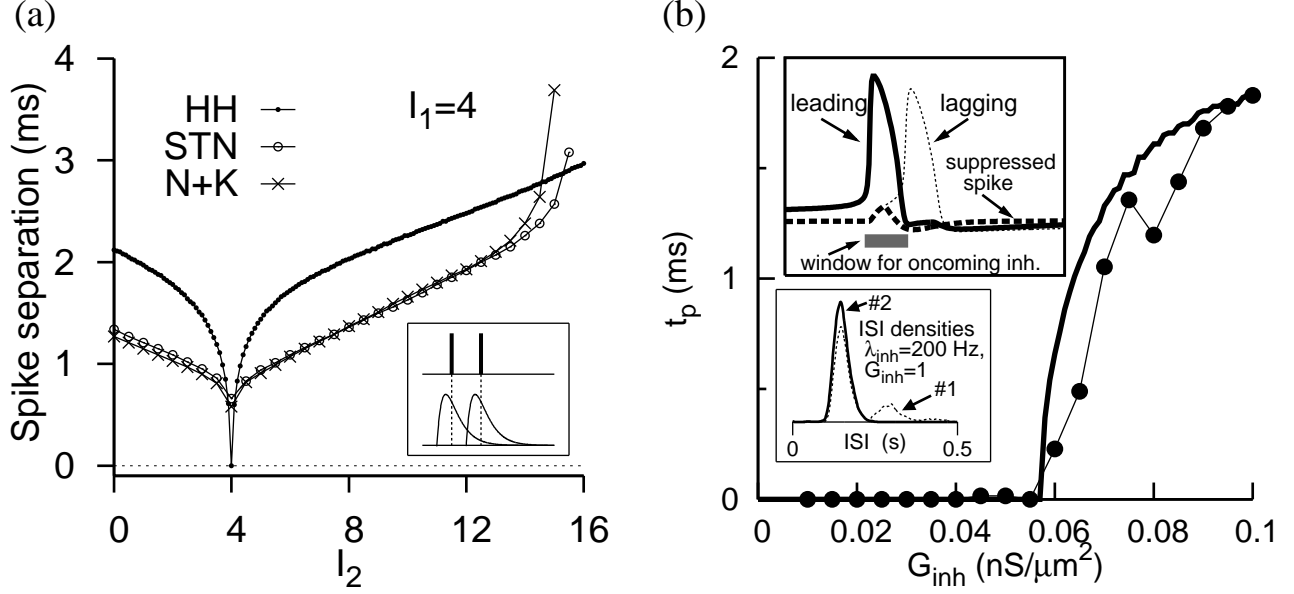


FIG. 2: (a) Time window of spike separation in 1:1 phase-locked state in the absence of extrinsic input for the coupled STN, N+K and HH excitatory neuronal pairs as a function of frequency heterogeneity (I_1 is fixed at $4 \text{ pA}/\mu\text{m}^2$ for STN and N+K, and at $4 \mu\text{A}/\text{cm}^2$ for the HH.) The inset shows scenarios of input events with respect to spike pair separation discussed in the text. (b) Excitatory STN network. Predicted and computed time windows (see text). The top inset shows the mechanism by which oncoming inhibition suppressed a lagging spike. The bottom inset shows the resultant interspike interval histogram densities. ($\tau_{inh} = 1 \text{ ms}$, $g_{exc} = 0.5 \text{ nS}/\mu\text{m}^2$.)

in a time window t_p (smaller or bigger than t_w) with respect to, but preceding the onset of the excitatory postsynaptic conductance, can eliminate the stimulated spike in the lagging neuron. A is a measure of the probability of such a favorable window receiving one or more inhibitory stimuli ($1 - P_0(\lambda_{inh}, t_p)$, where $P_n(\lambda, t)$ is the Poisson probability density) that successfully eliminate the following spike. Assuming a successful elimination of the secondary spike by one or more arriving inputs in a window, and assuming $t_p \approx t_w$, we write $A = Q(1 - e^{-\lambda_{inh}t_w})$, where Q is a constant that depends on the phase-locked frequency. $dA/d\lambda_{inh} = Qt_w e^{-\lambda_{inh}t_w}$. Q was estimated numerically from $dA/d\lambda_{inh}$. At $G_{inh} = 0.1 \text{ nS}/\mu\text{m}^2$ and $t_w = 1.8 \text{ ms}$, $Q = 0.034$. By using Q , and the numerically evaluated $dA/d\lambda_{inh}$, we solved the above transcendental equation for t_w at several G_{inh} values, and plotted it as t_p in Fig. 2(b), in dots. A similar window for suppression of the lagging spike is computed deterministically by using an inhibitory conductance input preceding the phase-locked spike

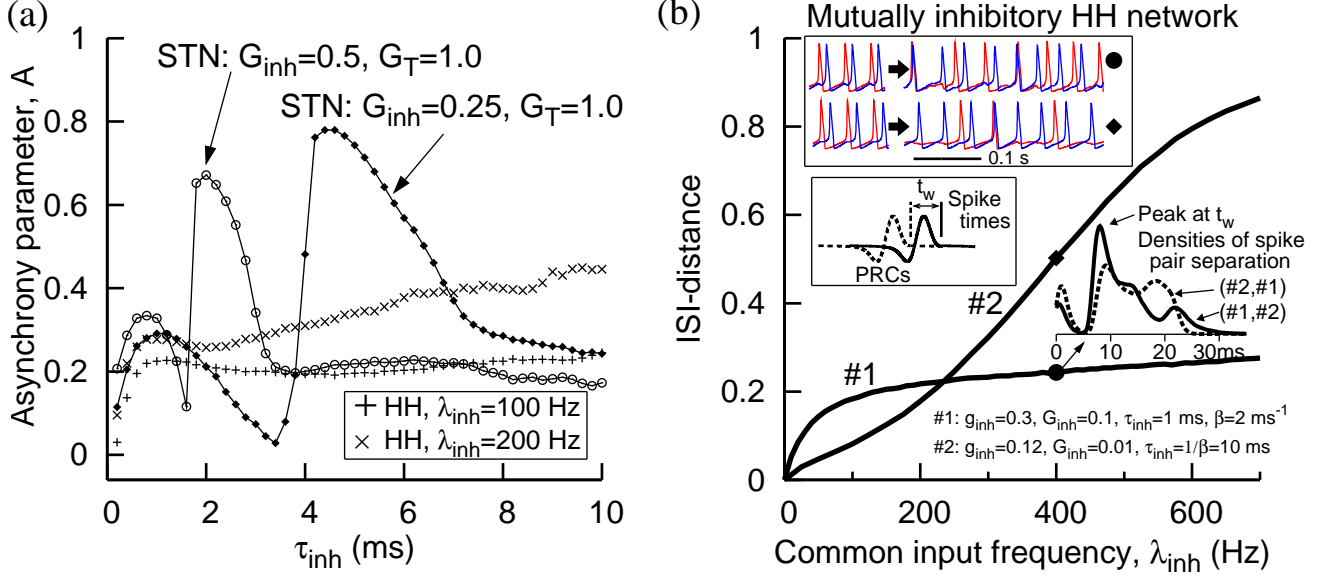


FIG. 3: (a) Dependence of A on τ_{inh} . For STN network $\lambda_{inh} = 100$ Hz, $g_{exc} = 0.5$ nS/ μm^2 . For HH network $G_{inh} = 0.5$ mS/ cm^2 and $g_{exc} = 0.1$ mS/ cm^2 . I_1 and I_2 are as in Fig. 1(b). $1/\beta = 3$ ms for both the networks. (b) Mutually inhibitory network of two coupled HH neurons ($I_1 = 0$, $I_2 = 8$ $\mu\text{A}/\text{cm}^2$) displaying spike time asynchrony for inhibitory input. At $\lambda_{inh} = 0$, $t_w = 7.8$ for #1 and 9.6 ms for #2. Voltage traces transitioning from phase-locked ($\lambda_{inh} = 0$) to asynchronous state for finite input rate are illustrated in the top inset. The phase response curves corresponding to the two phase-locked neurons are illustrated in the left inset, bottom. The right inset shows the densities of spike pair separation in the asynchronous state.

pair, and is shown in Fig. 2(b) (thick solid line) for comparison. Alternatively, A may be approximated. Such an approximation even at large G_{inh} values well predicts the growth of A [Fig. 1(b), STN, analytic] at small λ_{inh} : $A = 1.02 (1 - e^{-0.002\lambda_{inh}})$. Using a similar approximation for the HH network [Fig. 1(b), HH, analytic] yields $A = 1.8 (1 - e^{-0.0026\lambda_{inh}})$. For basal ganglia networks, values of τ_{inh} are near 10 ms. Increasing τ_{inh} generally decreased the firing rates in the models because the input turned increasingly deterministic, and the asynchrony parameter showed a moderate increment [Fig. 3(a)]. But the STN network showed up to 80% loss of phase-locked spike pairs when G_{inh} is reduced appropriately at long τ_{inh} such that the cells could maintain high firing rates due to activated T-current. The modulation in A is similar in nature to that seen in Fig. 1(b).

We now briefly discuss the behavior of mutually inhibitory HH neurons [Fig. 3(b)] in

response to common external Poisson inhibition. Phase-locking can now occur in such networks with t_w near the anti-phase state. t_w is modified by the frequency heterogeneity. This phase difference between the spikes is either decreased or increased by the occurrence of oncoming inhibitory synaptic conductance events before or in between the phase-locked spike pair. This increased the asynchrony as measured by the ISI-distance (defined earlier) with increasing λ_{inh} at fast as well as slow synaptic time constants, $1/\beta$. Finally, we illustrate the manifestation of these two forms of asynchrony in a larger network ($N = 10$) of excitatory [STN, all-to-all coupled; $n = 9$; Fig. 4(a)] and inhibitory [HH, sparse coupled; $n = 4$; Fig. 4(b)] neurons. The current balance equations are $\dot{V}_j = I_j - I_g^j - g \frac{1}{n} \sum_{k=1}^N M_{jk} S_k \times (V_j - E) - I_{\text{inh}}(V_j, t)$, $j = 1, \dots, 10$. $M_{jj} = 0$. $M_{jk} = 1$, if the presynaptic neuron k is connected to the postsynaptic neuron j , and 0 otherwise. In both the networks, in the absence of the input, the spike times were asynchronous for weak coupling (see [30] for T-current induced clustering), but strong mutual coupling above a critical level synchronized the average firing rates of all the neurons to a common frequency. When the shared inhibition is turned on, the STN network neurons fired faster due to T-current activation, and the HH network neurons fired slower. But the average firing rates exhibited asynchrony by diverging from the common locked frequency.

In contrast to the earlier studies on weakly coupled oscillator theory, we showed that in strongly coupled heterogeneous networks, shared inhibition can lead to asynchrony of spike times. Our simulations also revealed similar role for shared excitation. Our results lead to the possibility that modulating the synaptic input strength or input frequency might lead to switches in the synchrony-asynchrony (or coherence-incoherence) transitions in coupled oscillatory networks that receive coherent input. It would be of interest to study the emergence of asynchrony due to shared inputs when the phase-locked state is affected by background noise [31] or if the oscillators themselves behave chaotically [32]. In Parkinsonian network models of deep brain stimulation, earlier studies [33, 34] relied on the network connectivity between different brain nuclei to produce complex asynchronous patterns. Our results suggest of an alternative mechanism for generating such asynchrony within each brain nucleus.

We thank the Computational Biology Initiative (UTHSCSA/UTSA) and Texas Advanced Computing Center (TACC), The University of Texas at Austin for providing high performance computing resources. The work was supported by NIH/NINDS NS47085.

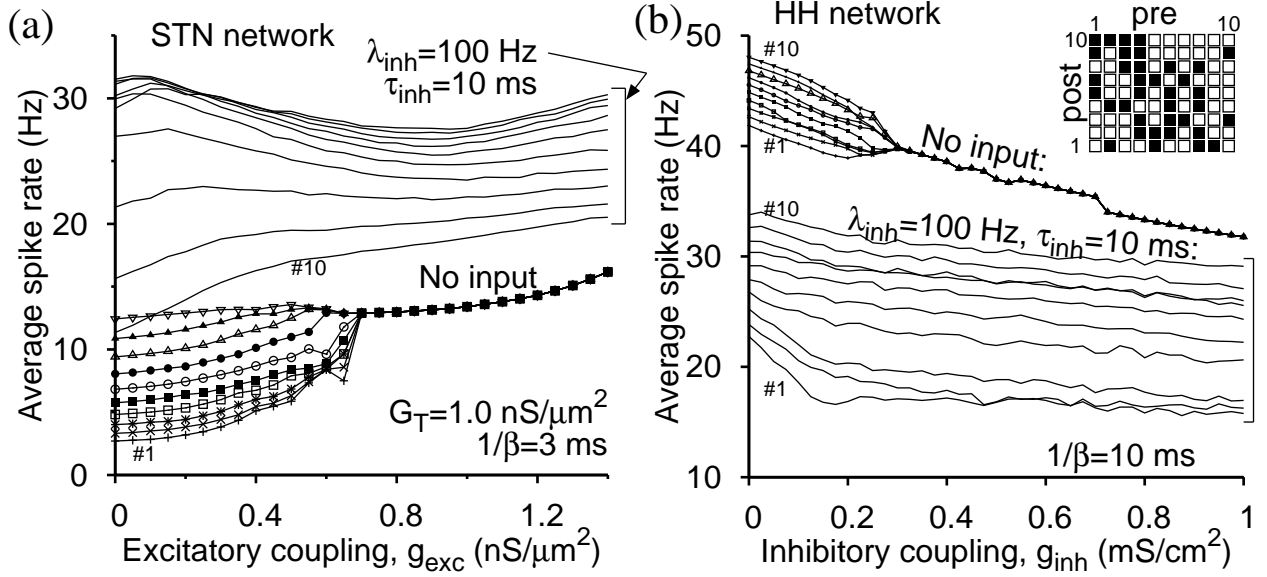


FIG. 4: Emergence of asynchrony from coherent states in networks of $N = 10$ excitatory all-to-all coupled STN (a) and sparsely coupled inhibitory HH (b) neurons measured by average spike rate as a function of mutual coupling without and with shared inhibition. (a) $I_j = (j - 1)10/9 \text{ pA}/\mu\text{m}^2$, $j = 1, \dots, N$, and $G_{\text{inh}} = 0.5 \text{ nS}/\mu\text{m}^2$. (b) Inset shows M_{ij} (with $n = 4$); a filled square represents a synaptic connection. $I_j = 5 + (j - 1)8/9 \mu\text{A}/\text{cm}^2$, $j = 1, \dots, N$, $G_{\text{inh}} = 0.1 \text{ mS}/\text{cm}^2$.

-
- [1] S. H. Strogatz, *Physica D* **143**, 1 (2000).
 - [2] H. Hong, H. Chaté, H. Park, and L.-H. Tang, *Phys. Rev. Lett.* **99**, 184101 (2007).
 - [3] Y. Kuramoto, *Chemical Oscillations, Waves and Turbulence* (Springer, Berlin, 1984).
 - [4] A. T. Winfree, *The Geometry of Biological Time* (Springer, New York, 1980).
 - [5] Y. Tsubo, J. nosuke Teramae, and T. Fukai, *Phys. Rev. Lett.* **99**, 228101 (2007).
 - [6] Y. Kuramoto and I. Nishikawa, *J. Stat. Phys.* **49**, 569 (1987).
 - [7] D. Hansel, G. Mato, and C. Meunier, *Neural Comput.* **7**, 307 (1995).
 - [8] J. G. Mancilla, T. J. Lewis, D. J. Pinto, J. Rinzel, and B. W. Connors, *J. Neurosci.* **27**, 2058 (2007).
 - [9] T. J. Lewis and J. Rinzel, *J. Comp. Neurosci.* **14**, 283 (2003).
 - [10] X.-J. Wang and G. Buzsáki, *J. Neurosci.* **16**, 6402 (1996).
 - [11] P. H. E. Tiesinga and J. V. José, *J. Comp. Neurosci.* **9**, 49 (2000).

- [12] C. van Vreeswijk, L. F. Abbott, and G. B. Ermentrout, *J. Comp. Neurosci.* **1**, 313 (1994).
- [13] H. Y. Jeong and B. Gutkin, *Neural Comput.* **19**, 706 (2007).
- [14] J.-n. Teramae and D. Tanaka, *Phys. Rev. Lett.* **93**, 204103 (2004).
- [15] Y. Kawamura, H. Nakao, K. Arai, H. Kori, and Y. Kuramoto, *Phys. Rev. Lett.* **101**, 024101 (2008).
- [16] F. C. Hoppensteadt and E. M. Izhikevich, *Weakly Connected Neural Networks* (Springer-Verlag, New York, 1997).
- [17] M. D. Bevan and C. J. Wilson, *J. Neurosci.* **19**, 7617 (1999).
- [18] P. C. Matthews and S. H. Strogatz, *Phys. Rev. Lett.* **65**, 1701 (1990).
- [19] J. A. White, C. C. Chow, J. Ritt, C. Soto-Trevino, and N. Kopell, *J. Comp. Neurosci.* **5**, 5 (1998).
- [20] L. Neltner, D. Hansel, G. Mato, and C. Meunier, *Neural Comput.* **12**, 1607 (2000).
- [21] M. D. Binder and R. K. Powers, *J. Neurophysiol.* **86**, 2266 (2001).
- [22] C. Ly and G. B. Ermentrout, *J. Comp. Neurosci.* (2008), doi:10.1007/s10827-008-0120-8.
- [23] A. Raz, E. Vaadia, and H. Bergman, *J. Neurosci.* **20**, 8559 (2000).
- [24] D. Golomb and D. Hansel, *Neural Comput.* **12**, 1095 (2000).
- [25] S. J. Schiff, P. So, T. Chang, R. E. Burke, and T. Sauer, *Phys. Rev. E* **54**, 6708 (1996).
- [26] K. Pyragas, *Phys. Rev. E* **54**, R4508 (1996).
- [27] C. Koch, *Biophysics of Computation* (Oxford University Press, Oxford, 1999).
- [28] X.-J. Wang and J. Rinzel, *Neural Comput.* **4**, 84 (1992).
- [29] T. Kreuz, J. S. Haas, A. Morelli, H. D. I. Abarbanel, and A. Politi, *J. Neurosci. Methods* **165**, 151 (2007).
- [30] D. T. W. Chik, S. Coombes, and Z. D. Wang, *Phys. Rev. E* **70**, 011908 (2004).
- [31] L. C. Yu, Y. Chena, and P. Zhang, *Eur. Phys. J. B* **59**, 249 (2007).
- [32] M. G. Rosenblum, A. S. Pikovsky, and J. Kurths, *Phys. Rev. Lett.* **78**, 4193 (1997).
- [33] J. E. Rubin and D. Terman, *J. Comp. Neurosci.* **16**, 211 (2004).
- [34] X.-J. Feng, E. Shea-Brown, B. Greenwald, R. Kosut, and H. Rabitz, *J. Comput. Neurosci.* **23**, 265 (2007).
- [35] D. Terman, J. E. Rubin, A. C. Yew, and C. J. Wilson, *J. Neurosci.* **22**, 2963 (2002).
- [36] See [35] for the original formulation. $dx_j/dt = (x_\infty(V_j) - x_j)/\tau_x(V_j)$, where $x \equiv n, h$, and r ;
 $\frac{d[\text{Ca}]_j}{dt} = 3.75 \times 10^{-5}(-I_{\text{Ca}}(V_j) - I_T(V_j, r_j) - 22.5[\text{Ca}]_j)$, where $I_g(V_j, n_j, h_j, r_j, [\text{Ca}]_j) = I_L(V_j) +$

$I_{\text{Na}}(V_j, h_j) + I_K(V_j, n_j) + I_{\text{Ca}}(V_j) + I_T(V_j, r_j) + I_{\text{AHP}}(V_j, [\text{Ca}]_j)$, and $I_{\text{Na}}(V, h) = G_{\text{Na}} m_{\infty}^3(V) h \times (V - E_{\text{Na}})$, $I_K(V, n) = G_K n^4 \times (V - E_K)$, $I_L(V) = G_L \times (V - E_L)$, $I_{\text{Ca}}(V) = G_{\text{Ca}} s_{\infty}^2(V) \times (V - E_{\text{Ca}})$, $I_T(V, r) = G_T a_{\infty}^3(V) b_{\infty}^2(r) \times (V - E_{\text{Ca}})$, $I_{\text{AHP}}(V, [\text{Ca}]) = G_{\text{AHP}} [\text{Ca}] / ([\text{Ca}] + 15) \times (V - E_K)$. $m_{\infty}(V) = 1/[1 + e^{-(V+30)/15}]$, $h_{\infty}(V) = 1/[1 + e^{-(V+39)/3.1}]$. $n_{\infty}(V) = 1/[1 + e^{-(V+32)/8}]$, $s_{\infty}(V) = 1/[1 + e^{-(V+39)/8.0}]$. $r_{\infty}(V) = 1/[1 + e^{(V+67)/2}]$, $a_{\infty}(V) = 1/[1 + e^{-(V+63)/7.8}]$, and $b_{\infty}(r) = 1/[1 + e^{-10(r-0.4)}] - 1/[1 + e^4]$. $\tau_n(V) = \frac{4}{3}[1 + \frac{100}{1+e^{(V+80)/26}}]$, $\tau_h(V) = \frac{4}{3}[1 + \frac{500}{1+e^{(V+57)/3}}]$, $\tau_r(V) = 5[40 + \frac{17.5}{1+e^{(V-68)/2.2}}]$. $E_L = -60$ mV, $E_K = -80$ mV, $E_{\text{Na}} = 55$ mV, and $E_{\text{Ca}} = 140$ mV. $G_L = 2.25$ nS/ μm^2 , $G_K = 45$ nS/ μm^2 , $G_{\text{Ca}} = 0.5$ nS/ μm^2 , $G_{\text{Na}} = 37.5$ nS/ μm^2 , $G_T = 0.5$ nS/ μm^2 , and $G_{\text{AHP}} = 9.0$ nS/ μm^2 .

[37] $S(V_j, t)$ evolves according to $dS(V_j, t)/dt = 4/(1 + e^{-(V_j - \theta_{\text{syn}})/k_{\text{syn}}})[1 - S(V_j, t)] - \beta S(V_j, t)$, where $\theta_{\text{syn}} = -20$ mV, $k_{\text{syn}} = 2$ mV. When unspecified, $\beta = 2$ ms $^{-1}$ in all networks.